Analytical Methods

ROYAL SOCIETY OF CHEMISTRY

PAPER

View Article Online
View Journal | View Issue

Cite this: *Anal. Methods*, 2022, **14**, 4077

Dy(III)-coordination imprinted self-assembly microspheres based on a silica core for highly sensitive and selective detection of two carbamate pesticides†

Zerong Long, *[a] Shilin Shen[ab] and Hui Yuan[a]

Carbamate (CB) pesticides possess potential carcinogenic and mutagenic activities towards humans even at very low dosages. Thus, broad-specificity probes with high sensitivity and speed are needed for multiple CB determination. This study is the first to focus on Dy^{3+} ions-coordinated self-assembly on a silica core using a surface imprinting procedure, for the simultaneous fluorometric detection of residues of metolcarb (MC) and pirimicarb (PC) insecticides. A simple and mild solvothermal method was applied for the preparation of fluorescent imprinted microspheres starting from 1,10-phenanthroline (Phen)-ligated Dy^{3+} ions to guide imprinted self-assembly of chitosan (CTS), glutaraldehyde (GA), and two carbamate pesticides (MC and PC) on the silica surface by means of coordinate bonds and hydrogen bonds. The as-prepared microspheres displayed strong fluorescence emissions *via* the antenna effect derived from the Phen ligand and the Schiff base oligomers for sensitizing the Dy^{3+} ions. An expanded in-depth mechanism study was performed on the fluorescence enhancement involving Förster resonance energy transfer (FRET) from the pesticides (donor) to the acceptor. A linear increase in fluorescence at 483 nm for MC and 574 nm for PC upon the imprinted microspheres was observed under the same 350 nm excitation wavelength. Moreover, the quantitative recognition process could be carried out simultaneously and tolerate strong distractions both from five other similar carbamate insecticides and from complicated matrices (*e.g.*, an extract of *Chrysanthemum morifolium* Ramat). The detection limit was 4 ng mL^{-1} with a range of 10–60 ng mL^{-1} for MC and 0.4 ng mL^{-1} with a range of 1–30 ng mL^{-1} for PC. Further characterization of the material, including TEM, SEM, XPS, and FTIR, Raman, and fluorescence spectra,

Received 9th August 2022
Accepted 17th September 2022

DOI: 10.1039/d2ay01269c

rsc.li/methods

[a]*State Key Laboratory of Market Supervision, Xinjiang Uygur Autonomous Region Product Quality Supervision and Inspection Institute, Urumqi, China. E-mail: long8326rong@163.com*

[b]*School of Chinese Pharmacy, Xinjiang Medical University, Urumqi, China*

† Electronic supplementary information (ESI) available. See https://doi.org/10.1039/d2ay01269c

Zerong Long received her PhD (2010) from Lanzhou Institute of Chemical Physics (LICP), Chinese Academy of Science (CAS). After completing post-doctoral research at the School of Chemistry and Chemical Engineering, Xinjiang University, she joined the Xinjiang Uygur Autonomous Region Product Quality Supervision and Inspection Institute, where she is currently a professor-level senior engineer. Her research focuses on the design and preparation of new functional nanomaterials and their sensing application in chemical and biological fields.

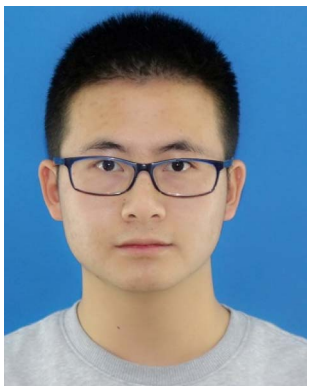

Shilin Shen is a graduate student at Xinjiang Medical University and his current researches include analysis of traditional Chinese medicine and agricultural products.

verified that the Dy^{3+} ions play a decisive role in promoting imprinted self-assembly around the silica core. Hence, a novel polynuclear Ln–organic imprinted probe having high selectivity, stability, and sensitivity for the detection of two carbamate insecticides is presented in this study.

Introduction

Polymetallic lanthanide ion (Ln^{III})-organic ensembles are a fast-growing and intriguing research field owing to their unique photophysical, catalytic, magnetic, and coordination properties.[1–5] In these lanthanide (Ln = Sm, Eu, Tb, Nd, Dy, and Yb) complexes, suitable organic ligands containing strong chromophores (*e.g.*, 1,10-phenanthroline, acyclic bis-tetradentate 1,29-dialdehyde, *etc.*) can sensitize the visible emission of lanthanide ions by the "antenna effect".[1,3,4] Moreover, polynuclear Ln-structures, including tetrahedron, helicate, metallacycle, metallacage, and porous metal–organic framework (MOF), showed extremely sharp luminescence emission and excellent mechanical strength,[3–5] which are considered desirable for the further development of luminescent recognition devices. For instance, lanthanide-MOFs with accessible pores and intrinsic luminescence can capture the title analytes (*e.g.*, Fe^{3+}, Cu^{2+}, Eu^{3+}, Dy^{3+}, MnO_4^-, $Cr_2O_7^{2-}$, *etc.*) and produce a host–guest combination signal in terms of detectable luminescence changes.[6–10] However, luminescence detection of complicated organic guests still represents a great challenge owing to the inherent deficiencies of the restricted capacity of the cavities and poor binding sites in these polynuclear lanthanide complexes. Fortunately, such Ln^{III}-organic luminescent ensembles with distinct inner spaces and diverse functional sites can be modified by interpenetrating inorganic salts,[11] grafting organics,[12] and depositing polymers[13,14] for sensing complicated organic molecules.

Surface-imprinted polymers have proven to be rapid and specific molecular recognition materials with the capacity for tailor-made flexibility and spatial prearrangement.[15,16] Moreover, large specific recognition areas, swift binding kinetics, short analysis times, and easy template removal enable successful detection of pesticides,[17,18] fungicides,[19,20] glucose,[21] viruses,[22] and proteins[23,24] using surface-imprinted widgets. Recently, an MOF-based surface-imprinted probe was prepared by imprinting hepatitis A virus (HAV) onto the surface of a pH-responsive metal–organic framework (MIL-101) for selective determination of the templates within 20 min through resonance light scattering (RLS) with a linear response to concentrations of 0.02–2.0 nmol L^{-1} and a limit of detection (LOD) of 0.1 pmol L^{-1}.[22] The work combined the advantages of surface-imprinting (accessible for targets) and a metal–organic framework (rigid skeleton, large specific surface area, and sensitive light transduction) for quick sensing recognition of viruses. In addition, terbium(III) ions complexed with *N*-methacryloyl-L-histidine (MAH) were assembled directly into the imprinted polymeric backbone, realizing highly efficient chiral separation and fluorescent monitoring of proteins.[24] The polynuclear Ln–organic imprinted probe displayed high fluorescence intensity, strong mechanical stability, and accurate identification for L-histidine; nevertheless, only individual cases have been reported as far as we know.

Herein, we report a new polynuclear Ln–organic probe *via* the introduction of dysprosium(III) ions into imprinted copolymerization through coordination self-assembly based on a silica core for sensitive fluorometric detection of the insecticides metolcarb (MC) and pirimicarb (PC). In detail, Dy^{3+} ions ligated to 1,10-phenanthroline (Phen) according to a 1 : 1 molar ratio were coated on the surface of silica nanoparticles (NPs), around which the coordination-unsaturated Dy^{3+} then further directed the assembly of chitosan (CTS), glutaraldehyde (GA) and two templates (MC and PC) under mild experimental conditions; it is noteworthy that Phen ligand and Schiff base oligomers acted as antennas to sensitize Dy^{3+} ions even after they had been embedded in the imprinting layer. Moreover, the as-prepared composites consisted of highly dispersed smooth microspheres with a uniform diameter. Furthermore, recognition of the templates by the new probe was simultaneously carried out in mixed MC and PC solution using two completely independent emissions (blue emission at 483 nm for MC and yellow at 574 nm for PC) under the same excitation (350 nm) within 10 min. Additionally, the fluorescent probe displayed an excellent linear fluorescence correlation against different concentrations of MC and PC with rather low detection limits. The novelty of this investigation rests on the Dy(Phen) complex guided imprinted self-assembly around the SiO_2 core by coordinate bonds and hydrogen bonds to build a robust 3D polymetallic backbone with luminescent dual emission centers as the recognition component of the sensor. Thus, molecular recognition and signal transduction could be performed in reciprocal independent emission channels in the process of sensing detection for accurate and rapid MC and PC quantification.

Yuan Hui received her Master's degree in biochemistry and molecular biology from Xinjiang Agricultural University in 2009. From 2009 to the present, she has engaged in the inspection of food, agricultural products and light-industry products in the Xinjiang Uygur Autonomous Region Product Quality Supervision and Inspection Institute, where she is currently a positive-senior experimentalist.

Experimental

Chemicals and materials

Dysprosium(III) nitrate pentahydrate ($Dy(NO_3)_3 \cdot 5H_2O$, 99.99%, Energy Chemical, Saen Chemical Technology (Shanghai) Co.),

1,10-phenanthroline (Phen, 98%, Shanghai Aladdin Biochemical Technology Co.), methanol (AR, Tianjin Fuyu Chemical Technology Co.), acetic acid (AR, Tianjin Baishi Chemical Technology Co.), anhydrous ethanol (AR, Tianjin Zhiyuan Chemical Technology Co.), tetraethyl orthosilicate (TEOS, 99.99%, Tianjin Yongcheng Fine Chemicals Co.), ammonia aqueous solution (25–28 wt%, Chengdu Aikeda Chemical Reagent Co.), chitosan (CTS, 85% deacetylation, Shanghai Aladdin Bio-Chemical Technology Co.) and glutaraldehyde (GA, 50 wt%, Shanghai Aladdin Bio-Chemical Technology Co.) were used. Pirimicarb (PC, 98.8%), metolcarb (MC, 99%), methomyl (MT, 98.5%), isoprocarb (IP, 99.4%), carbofuran (CF, 98.8%), carbaryl (CB, 99.4%) and aldicarb (AD, 99.5%) were purchased from Shanghai Pesticide Research Institute. Silica nanoparticles were prepared following the previously reported Stöber method.[25] Distilled water and ultrapure water were prepared using a Milli-Q system (Millipore Corporation, USA).

Apparatus and conditions

Fluorescence spectra were determined using a Model F-4500 spectrophotometer (Hitachi, Japan). Ultraviolet-visible (UV-vis) absorption spectra were recorded on a UV-2450 UV-vis spectrofluorometer (Shimadzu, Japan). Fourier transform infrared (FTIR) spectra were measured in KBr using Vertex70 equipment (Bruker, Germany). The surface elemental composition of the composite SiO_2@Dy(Phen)-imprinted NPs was characterized using an ESCALAB-250Xi X-ray photoelectron spectrometer (aluminum target, Thermo Fisher Scientific, USA). SiO_2@Dy(Phen)-imprinted NPs were characterized using transmission electron microscopy (TEM; H-600, accelerating voltage 100 kV, Hitachi, Japan) and GEMINI300 scanning electron microscopy (Zeiss, USA). Time-resolved fluorescence spectra were measured using an FL1000 spectrometer [time-correlated single-photon counting (TCSPC) system, Edinburgh Analytical Instruments, UK]. Raman spectra were obtained by using a laser confocal Raman spectrometer (Dxr2xi, Thermo Fisher Scientific, USA). A DF-101S heat-collecting magnetic heating stirrer, a B11-3 thermostatic magnetic stirrer, a ZF-2 three-use ultraviolet lamp, a D2012 personal high-speed microcentrifuge, a GM200 Grindomix, and a JP-070S ultrasonic instrument were used in the experimental procedure; these were purchased from Jiangsu Jincha Instrument Technology Co., China, Shanghai Sile Instrument Co., China, Shanghai Anting Electronic Instrument Factory, China, Scilogex, USA, Retsch, Germany, and Skymen, China, respectively. X-ray photoelectron spectroscopy (XPS) standard binding energies were determined following the Handbook of monochromatic XPS spectra: the elements and native oxides, XPS International, Wiley.[26]

Synthesis of SiO_2@Dy(Phen) NPs

First, 1.5 mmol (725.4 mg) $Dy(NO_3)3\cdot 5H2O$ and 1.5 mmol (297.3 mg) Phen were together dissolved in 50 mL anhydrous ethanol, then refluxed gently with stirring at 70 °C in an oil bath for 4 h. Subsequently, the mixed solution was allowed to stand at ambient temperature for 24 h and a pale-pink powder was obtained. The synthesized Dy(Phen) complex was washed with anhydrous ethanol several times to reach neutrality, repeatedly centrifuged at 4834 g for 15 min, and stored in a refrigerator at 4 °C for further use.

Then 1.5 g white colloidal SiO_2 particles were mixed with 0.6 g Dy(Phen) and 5 mL deionized water. The mixture was transferred to an agate mortar and ground clockwise until it became a paste. It was then dried in an air oven at 110 °C for about 8 h and white powdery nanospheres were finally harvested.

Synthesis of composite SiO_2@Dy(Phen)-MIP NPs

First, 0.25 g CTS was added into 50 mL acetic acid (2 wt%) solution with ultrasonic dispersion for 30 min to obtain a transparent solution, followed by the addition of 0.2 g SiO_2@Dy(Phen) NPs into the above-mentioned solution for another 30 min of ultrasonic stirring. Thereafter, the mixture was stirred at 65 °C (oil bath) for 16 h and centrifuged at 4834 g for 15 min. Then the obtained CTS-modified SiO2@Dy(Phen) powder was repeatedly washed with distilled water and anhydrous ethanol to reach neutral pH, repeatedly centrifuged at 4834 g for 15 min, and vacuum dried at 40 °C for 4 h.

Assembling of the imprinted polymer shell at the surface of CTS-modified SiO_2@Dy(Phen) microspheres was performed according to the following procedure. Then, 100 mg as-prepared CTS-modified SiO_2@Dy(Phen) microspheres, 80 mg PC, and 56 mg MC were dispersed together into 50 mL anhydrous ethanol and stirred gently overnight at room temperature to form the preassembly solution, into which 1 mL 25 wt% GA was then added. The reaction mixture was vigorously stirred at 40 °C (oil bath) for 6 h and then the temperature was further raised to 70 °C and maintained there for 2 h, producing a uniform and compact dual-template imprinted polymer at the surface of SiO2@Dy(Phen) NPs. The composite polymer microspheres were eluted with methanol/acetic acid (85 : 15, v/v) to remove the excess templates, and washed with methanol several times until at neutral pH. The obtained dual-template molecularly imprinted polymers (DMIPs) were dried in a vacuum drying oven and stored at ambient temperature. For comparison, two single-template imprinted polymers (MC-MIPs and PC-MIPs) and the non-imprinted composite polymers (NIPs) were also prepared and rinsed under identical experimental conditions, except that only one template (MC or PC) or none at all was used in the reaction process.

Fluorescent characterization of composite MIP NPs

In the experiments, the influence of shaking time on fluorescence enhancement efficiency was also studied. In brief, 2 mg DMIPs were evenly dispersed into 2 mL anhydrous ethanol to obtain a translucent colloid solution, then mixed with a 50 μL ethanol solution of PC and MC at a concentration of 2 μg mL^{-1} in a 5 mL centrifuge tube. The mixed solution was incubated for regular time intervals from 1 to 15 min at ambient temperature and the fluorescence intensities at 483 nm and 574 nm were detected every 1 min for a single excitation wavelength of 350 nm. Similarly, two single-template imprinted polymers were subjected to the same procedure to investigate the dependence of their fluorescence enhancement upon shaking period.

Subsequently, the simultaneous quantitative analysis of PC and MC by means of the DMIPs was evaluated. The fluorescence

spectra of DMIPs with different concentration gradients of PC and MC were investigated to analyze their sensitivity.

Herein, 2 mL ethanol colloidal solution containing 2 mg DMIPs was mixed with PC and MC at a concentration of 2 μg mL^{-1} in different volumes (1, 2, 4, 6, 8, 10, 20, 30, 40, 50, and 60 μL) in 5 mL centrifuge tubes. Then these samples were incubated at room temperature for 10 min and the fluorescence emission spectrum of each centrifuge tube was determined at 483 nm and 574 nm under the excitation of 350 nm. In addition, two single-template imprinted polymers were analyzed in the same way under identical conditions.

To evaluate the specific selectivity of DMIPs, 50 μL of ethanol solution containing 2 μg mL^{-1} of PC and MC was mixed with 2.0 mL of a colloidal ethanol solution containing 2 mg dispersed DMIPs in a 5 mL centrifuge tube, shaking for 10 min in the ambient environment. The experimental procedure was repeated for the analogs CF, CB, AD, IP, and MT of PC and MC under the same conditions. The fluorescence intensity of each mixed group was individually recorded at 483 nm and 574 nm. Simultaneously, the NIPs were also used in the competitive identification experiments as a comparison with DMIPs.

Simultaneous determination of MC and PC in real samples

Dried *Chrysanthemum morifolium* Ramat samples were purchased from the local drugstore in Urumqi. The selected samples were exclusively free of PC and MC, and the spiking concentrations used were 15.0, 35.0, 55.0 ng mL^{-1} for MC (*A*) and 2.0, 10.0, 25.0 ng mL^{-1} for PC (*B*) according to an $A + B$ pattern with a one-to-one correspondence (such that $A + B = 15.0 + 2.0$, $35.0 + 10.0$, and $55.0 + 25.0$ ng mL^{-1}) in the spiked samples.

Here, accurately weighed 10.1 mg MC and PC were respectively dissolved in 20 mL absolute ethanol, transferred into 100 mL volumetric flasks, and made up to 100 mL to obtain reserve solutions with a concentration of 0.1 mg mL^{-1}. Three mixed standard solutions with PC concentrations of 1.5, 3.5, and 5.5 μg mL^{-1} and MC concentrations of 0.2, 1.0, and 2.5 μg mL^{-1}, respectively, were prepared. A weighed 10.0 g homogenized *Chrysanthemum morifolium* Ramat negative sample was placed in each of three beakers, 1 mL of mixed standard solution with different concentrations was added to each beaker, and afterward 50 mL ethanol was added and ultrasonic extraction was performed for 20 min. Then the sample was washed twice using *ca* 10 mL ethanol each time. Subsequently, each combined extracted solution was transferred to a 100 mL volumetric flask, diluted to the calibration mark with absolute ethanol, and allowed to stand for 2 h at ambient temperature. Then, 2.0 mg DMIPs were well dispersed in each spiked sample solution (2.0 mL) by shaking at 80 rpm for 10 min at ambient temperature. Fluorescence detection was carried out at 483 nm and 574 nm with 350 nm excitation.

Results and discussion

Surface morphology of SiO_2@Dy(Phen)-MIP NPs

Fig. 1 shows the synthetic route to the 3D-structured composite microspheres, SiO_2@Dy(Phen)-MIPs, under mild experimental

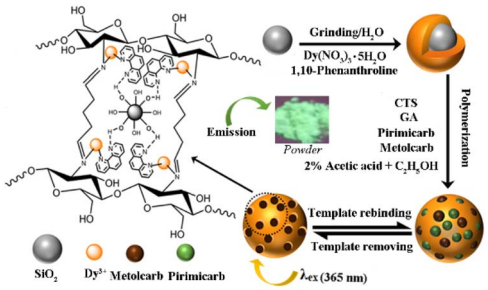

Fig. 1 Schematic illustration of the preparation of dual-template SiO_2@Dy(Phen)-MIPs (DMIPs). The inset shows bright yellow-green powder of DMIPs observed at 365 nm excitation under a three-use UV lamp.

conditions. In brief, 1,10-phenanthroline was ligated to Dy(III) cations at a ligand-to-metal molar ratio of 1 : 1, then attached to the surface of the base core of the SiO_2 by a hydrothermal method. Such composite nanospheres are highly sensitized *via* the optical antenna effect from ligand-mediated excitation, thereby obtaining prominent luminescent properties.[4] Subsequently, the imprinted polymer layer was assembled on the surface of SiO_2 by the coordination-unsaturated Dy^{3+} ions promoted copolymerization of CTS, GA, and two templates (MC and PC). The powder of SiO_2@Dy(Phen)-MIPs emits bright yellow-green photoluminescence (PL) under 365 nm excitation by using a three-use UV lamp.

Fig. 2 displays representative TEM images and SEM micrograph of the composite microspheres SiO_2@Dy(phen), SiO_2@Dy(Phen)@CTS, as well as dual-template SiO_2@Dy(Phen)-MIPs. As a result, the self-assembly process around the DMIPs from nano-SiO_2 to SiO_2@Dy(Phen)-MIPs NPs could be described according to the increasing average diameter of particles. SiO_2@Dy(Phen) NPs were seen to have uniform spherical morphology and homogenous metal distribution with negligible impurities as shown in Fig. 2a. Moreover, SiO_2@Dy(Phen)@CTS microspheres (Fig. 2b) were exclusively monodispersed and smooth without any defects. Not surprisingly, the dual-template SiO_2@Dy(Phen)-MIP NPs had an almost perfectly spherical, smooth, and milk-white appearance, as shown in Fig. 2c and d. Furthermore, the appearance of two single-template MIPs (Fig. S1†) was almost the same as that of

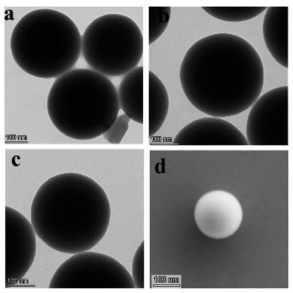

Fig. 2 TEM images of (a) SiO_2@Dy(Phen), (b) SiO_2@Dy(Phen)@CTS, (c) dual-template SiO_2@Dy(Phen)-MIPs (DMIPs), (d) SEM micrography of DMIPs nanoparticles.

DMIPs. The average diameter of these particles was *ca* 190, 210, and 230 nm, corresponding to SiO_2@Dy(phen), SiO_2@Dy(Phen)@CTS, and dual-template SiO_2@Dy(Phen)-MIP microspheres, respectively. The composite NPs have notable advantages for their strong PL emission and far lower price per unit mass (Dy, *ca* 6 wt%) in comparison with the pure phosphors.

Characterization of SiO_2@Dy(Phen)-MIP NPs

FTIR spectra of SiO_2@Dy(Phen)@CTS and SiO_2@Dy(Phen)@MIPs can be found in Fig. S2,† in which the characteristic bands at around 1102, 801, and 472 cm^{-1} are respectively attributed to Si–O asymmetrical stretching, symmetrical stretching, and bending vibrations, and that at *ca* 954 cm^{-1} to Si–O–H bending vibration.[25] Moreover, the wide band at 3424 cm^{-1} (Fig. S2a†) can be ascribed to the stretching vibrations of the hydroxyl and amino group from silicone, rare-earth hydrolysate, and CTS. As shown in Fig. S2b,† the characteristic peak at 1633 cm^{-1} can be assigned as the C=N stretching vibration caused by the aldimine condensation of CTS and GA. In comparison with Fig. S2a,† the band has moved about 77 cm^{-1} towards the low wavenumber position and is centered at 3348 cm^{-1} (Fig. S2b†), which is probably attributable to the disappearance of the amino group of CTS. This result indicates the hydrophilic copolymer came into being *via* the strong interaction force between CTS and GA at the surface of the SiO_2 base.

Raman spectra of DMIP powder along with the DMIP sample adsorbed with MC and PC are shown in Fig. S3.† The characteristic standard frequencies of Phen are 3065 (C–H), 1588 (C–N), 1446 (C=N), 1345 (δC–H), 1035 (ring) cm^{-1},[27] yet among these the stretching bands of C–N and C=N have moved to 1591 and 1457 cm^{-1}, respectively, in Fig. S3a.† This result shows that a coordinate bond was formed through Phen ligated to Dy^{3+} ions. Simultaneously, peaks are observed at 1259, 1056, 867, and 421 cm^{-1} which can be assigned as the ring stretching vibration of –CH and the bending vibration of C–H, as well as the symmetric stretching vibrations of C–O–C and C–C–O bonds of CTS.[28] The characteristic standard peak of the amino belonging to CTS at 3143 cm^{-1} has disappeared,[28] but a new band at 1628 cm^{-1} associated with imine (C=N) has appeared owing to the crosslinking between CTS and GA.[29] As compared with Fig. S3a,† the shift changes of all those peaks related to DMIPs are almost negligible after loading the templates (MC and PC). As a result, the specific band at 1727 cm^{-1} should be assigned as carbonyl bending vibration of CBs (Fig. S3b†). Unfortunately, the amount of Dy^{3+} ions in DMIPs is too low for their corresponding bands to be seen below 500 cm^{-1} in Fig. S3.†

Fig. S4† shows the X-ray photoelectron spectra of SiO_2@-Dy(Phen) and SiO_2@Dy(Phen). In Fig. S4a,† the characteristic peak at 1297.3 eV can be referred to Dy 3d5, which deviates about +1.1 eV from the handbook data (1296.2 eV). The photopeaks corresponding to O 1s (532.1 eV), C 1s (284.8 eV), and N 1s (399.0 and 406.5 eV) are completely derived from Phen. Also, the binding energy of N 1s is divided into two independent peaks, one of which is far higher than its standard value (398.4 eV). This result affords direct evidence that the Dy(III) ions are bonded to one of the nitrogen atoms given by Phen through coordination linkage; while the peak at 399.0 eV is supposed to be N 1s from the other nitrogen of Phen unligated to Dy^{3+} ions. For the composite DMIPs in Fig. S4b,† the binding energies of O 1s (532.1 eV) and C 1s (285.1 eV) are barely altered, but that of N 1s is split into three, at 399.0, 402.9, and 407.6 eV. Moreover, the characteristic peak of Dy $3d^5$ has moved +0.9 eV once again to arrive at 1298.2 eV. The imine C=N obtained through polymerization by CTS and GA most likely takes part in the coordination with the Dy(III) ions besides Phen. From what has been discussed above, it is sure that not only could Dy(Phen) ligated to the Schiff base oligomers further sponsor the spatial arrangement of CTS and GA in order, but also the unligated nitrogen atoms from Phen could bind to hydroxyl groups on the surface of silica by hydrogen bonds.

Binding properties of SiO_2@Dy(Phen)-MIP NPs

To our surprise, the typical emission peaks of DMIPs also kept the outstanding characteristic transitions of Dy^{3+} ions located at 483 nm for the $^4F_{9/2}$–$^6H_{15/2}$ blue band and 574 nm for $^4F_{9/2}$–$^6H_{13/2}$ yellow emission at 350 nm excitation although the Dy^{3+} ions were hidden in the imprinted layer.[30] Additionally, the emission intensity of DMIPs had been increased manifold owing to Phen and the Schiff base oligomers acting as antennas.[4,30] Stemming from this, we investigated the rebinding kinetics upon fluorescence emission of DMIPs using an initial concentration of 20 ng mL^{-1} mixture solution of MC and PC during a period of 1 to 15 min. As shown in Fig. 3, all of the single- or dual-template Dy(III)-coordination imprinted microspheres arrived at equilibrium adsorption within 10 min. Noticeably, there exists a close correlation between MC adsorption and the fluorescence intensity at 483 nm of DMIPs or MC-MIPs, as well as PC adsorption and the fluorescence intensity at 574 nm of DMIPs or PC-MIPs. Furthermore, the dynamic adsorption curve of DMIPs approached closely those of MC-MIPs and PC-MIPs at 483 and 574 nm emissions, respectively. Thus, it can be deduced that there is hardly any competitive adsorption between MC and PC for DMIPs even in a mixed solution of MC and PC at equal concentration.

As can be seen in Fig. 4, the fluorescence intensities of MIPs rose linearly at 483 nm with the addition of MC in the range of 10–60 ng mL^{-1} or at 574 nm for PC from 1 to 30 ng mL^{-1} in the

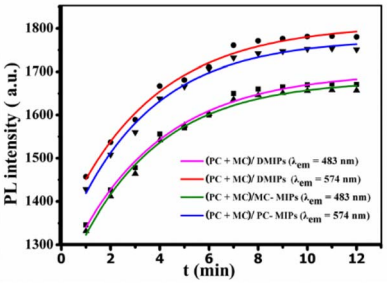

Fig. 3 Dynamic adsorption curves of single- and dual-template MIPs at different emission wavelengths (λ_{em} = 483 nm and λ_{em} = 574 nm) under the same excitation at 350 nm.

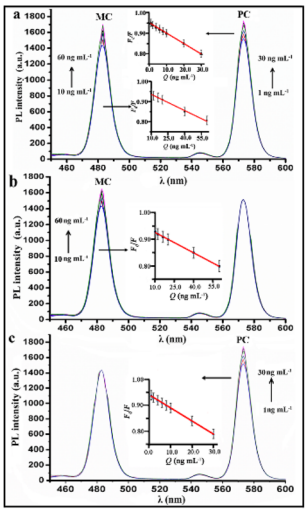

Fig. 4 Static adsorption curves of (a) DMIPs, (b) MC-MIPs and (c) PC-MIPs at different emission wavelengths (483 and 574 nm). The insets show the Stern–Volmer curves, where F and F_0 are the fluorescence intensities of MIPs in the presence and absence of templates.

mixed colloid nanospheres solution. The inset curves in Fig. 4 plotted using the Stern–Volmer equation,[25] describe the linear correlation between the fluorescence intensity (F_0/F, where F and F_0 are the fluorescence intensities of MIPs in the presence and absence of the template molecules, respectively; K_{sv} represents the enhancement constant of the analyte) and the concentration (Q) of MC or PC. Consequently, the static adsorption of DMIPs (Fig. 4a) was expressed as $F_0/F = 0.9633–0.0027Q$ ($R = 0.9944$) for MC with LOD of 4 ng mL^{-1} and a limit of quantification (LOQ) of 13 ng mL^{-1} within the range 10–60 ng mL^{-1}; the adsorption of DMIPs for PC was also linearly correlated, and the linear equation was $F_0/F = 0.9513–0.0051Q$ ($R = 0.9989$, LOD = 0.4 ng mL^{-1}, LOQ = 1.3 ng mL^{-1}) in the range of 1–30 ng mL^{-1}. Simultaneously, the static adsorption of two single-template imprinted NPs (MC-MIPs and PC-MIPs) was also investigated (Fig. 4b and c) by their fluorescence intensities *vs.* the concentrations of the corresponding analyte, *i.e.*, $F_0/F = 0.9519–0.0025Q$ ($R = 0.9986$, LOD = 4 ng mL^{-1}) in the range of 10 to 60 ng mL^{-1} for MC against MC-MIPs, and $F_0/F = 0.9413–0.0052Q$ ($R = 0.9937$, LOD = 0.4 ng mL^{-1}) in the range of 1–30 ng mL^{-1} for PC against PC-MIPs, respectively. It should be noted that the LOD and LOQ quoted are based on 3 and 10 σ/s ratios, where σ denotes the standard deviation from the blank solution and s represents the slope of the calibration curve. As shown in Fig. 4b and c, the single-template imprinted fluorescence NPs could detect their corresponding template molecules alone even in mixed MC and PC solution. However, DMIPs have extra merit on account of their accurate determination of MC and PC at the same time under the same excitation wavelength of 350 nm. As shown in Table S1,† the sensitivity of the broad-specificity DMIP sensor is close to that of the high-precision instrument method. As a result, the luminescent DMIP sensor is an alternative to other analytical methods and can be used for trace pesticide determination.

To further prove the resistance of DMIPs to interference from substances other than the templates, the control

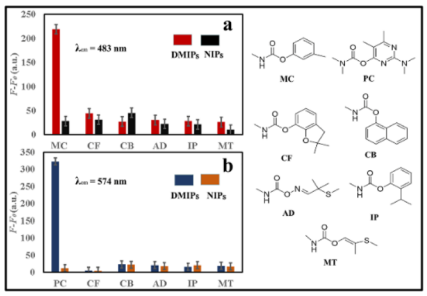

Fig. 5 The competitive adsorption capacity of seven analytes onto DMIPs and NIPs at different emission wavelengths ($\lambda_{em} = 483$ nm and $\lambda_{em} = 574$ nm).

experiments were adopted to observe the competition among the templates (PC and MC) and another five carbamate analogs (CF, CB, AD, IP, and MT) upon DMIPs. As shown in Fig. 5, the most noticeable fluorescence enhancement ($F–F_0$) was perceived after the templates MC and PC were added to the colloidal ethanol solution of DMIPs (Fig. 5a and b). In contrast, only subtle fluorescence changes of DMIP NPs were found on the addition of the other five analogs, at both 483 nm and 574 nm. Those analogs either possess a skeleton that closely resembles that of the templates (CF, CB, and IP) or merely contain the same chemical unit as the templates (AD and MT). The result showed those analogs could not be recognized by DMIPs. As a control, the fluorescence changes of NIP nanospheres upon addition of MC, PC, CF, CB, AD, IP, and MT were studied as well. Not surprisingly, the fluorescence intensities of NIPs barely changed at the addition of any one of these owing to the absence of recognition sites at the surface of NIPs. The control experiment provided concrete evidence of the specific recognition by DMIPs towards MC and PC with the assistance of the photoluminescence signal.

Analysis of fluorescence mechanism

Self-assemblies of luminescent rare earth compounds can strengthen their luminescent emission through donor–acceptor pairs, microcavities, enrichment of rare earth compounds, and shell protection against the environmental media.[2] As a result, it can be deduced that the increased emission of DMIPs in the presence of templates is most likely caused by the weak interaction between DMIPs and the templates and should not be arbitrarily referred to as 'the antenna effect'. Because we hardly observed any remarkable shift changes of DMIPs in their Raman spectrum or fluorescence spectra after adsorption of MC and PC, the fluorescence enhancement mechanism of DMIPs in the presence of templates was further investigated experimentally. As shown in Fig. S5a and b,†† the fluorescence emission spectrum of MC greatly overlapped with the UV-vis absorption and the excitation of DMIPs in the region 300 to 380 nm; while that of PC almost completely covered the absorption and the excitation spectra of DMIPs at 320–360 nm (Fig. S5c and d††). Generally, the Förster resonance energy transfer (FRET) depends largely on the relative direction of dipole–dipole pairs and the degree of the spectral overlap between the donor

Table 1 Recoveries and RSD at different spiking levels of the mixed MC and PC in *Chrysanthemum* samples ($n = 3$) measured by means of DMIPs

Sample	Analyte (A + B)	Determined?	Added A (ng mL^{-1})	Added B (ng mL^{-1})	Found (ng mL^{-1})	RSD (%, $n = 3$)	Recovery (%)
Chrysanthemum morifolium Ramat extract	MC + PC	Not found	15.0	—	12.94	1.07	86.2
			—	2.0	1.79	1.28	85.7
			35.0	—	33.32	2.42	92.2
			—	10.0	8.95	2.58	89.5
			55.0	—	50.21	1.06	91.3
			—	25.0	22.60	1.11	90.4

emission spectrum and the acceptor absorption spectrum.[31] The emission wavelength of MC (donor) deviated *ca* 20 nm from the excitation wavelength of DMIPs (acceptor), leading to a relatively difficult energy transfer from donor to acceptor. In contrast, FRET from PC to DMIPs was liable to occur because of the perfect overlap between the emission of PC and the excitation of DMIPs. This might give a reasonable explanation why the detection limit of PC is much lower than that of MC upon DMIPs. In addition, the fluorescence lifetimes of DMIPs (Table S2 and Fig. S6†) were prolonged from 38.4 to 58.5 μs for MC and from 57.7 to 98.3 μs for PC as the concentration of template rose from 0 to 30 ng mL^{-1}. The recognition sites at imprinted cavities consist of abundant hydroxyl groups, which can successfully capture directionally the templates by means of hydrogen bonds. Those hydrogen bonds can efficiently suppress the process of non-radiative decay of Dy^{3+} ions in the polymer network after excitation by ultraviolet irradiation, resulting in an extension of the fluorescence lifetime.[32] When the imprinted cavities are occupied by MC and/or PC during rebinding, a host–guest inclusion structured complex is formed and the fluorescence intensities produced by the Dy^{3+}-directed self-assembly system increased as the concentration of those pesticides is increased. Therefore, FRET between hosts and guests is considered to be responsible for the fluorescence enhancement of DMIPs.

Determination of MC and PC in real samples

Spiked recovery experiments were carried out to evaluate the practicality of using the DMIPs to detect MC and PC in an ethanol extract of *Chrysanthemum morifolium* Ramat. It should be noted that this extract contains multiple components, *e.g.*, *Chrysanthemum* flavonoids, essential oil, triterpenes, nonsteroidal phenols, polysaccharides, *etc.*, but not MC and PC. In this experiment, three mixed spiked concentrations of MC (A ng mL^{-1}) and PC (B ng mL^{-1}), where $A + B = 15.0 + 2.0$, $35.0 + 10.0$, and $55.0 + 25.0$, were used for recovery determination using DMIPs at 483 nm and 574 nm emission, respectively. The recoveries of MC were in the range of 86.2–92.2% with a relative standard deviation (RSD) of less than 3%, while PC recoveries were between 85.7% and 90.4% with lower than 3% RSD for all tested samples. Hence, ultra-trace detection in actual samples can be realized by means of the sensitive linear fluorescence response of DMIPs against MC and pirimicarb PC after a simple pretreatment (Table 1).

Conclusions

In this work, novel imprinted microspheres were prepared *via* Dy^{3+} ions self-assembling the imprinted polymer chain onto the surface of silica spheres. The polymerization occurs at each Dy^{3+} ion, thus avoiding the entanglement and overlap of those flexible polymer chains. The as-prepared self-assemblies displayed strong fluorescence emissions *via* the antenna effect driven by Phen and the Schiff base in the polymer backbone for sensitizing the Dy^{3+} ions. Such imprinted microspheres should have long-term fluorescence stability owing to their strong resistance to intrinsic disorder, denaturation, and backbone collapse. The imprinted microspheres had a sensitive and rapid fluorescence response to MC and PC at the same time with rather low detection limits. In addition, the Dy(Phen)-coordination imprinted self-assembly microspheres were successfully used for selective separation and fluorescent monitoring of insecticides metolcarb (MC) and pirimicarb (PC) in mixed spiked samples of an ethanol extract of *Chrysanthemum morifolium* Ramat, with recoveries over 85%.

Author contributions

Zerong Long: methodology, investigation, formal analysis, writing – original draft, and writing – review & editing. Shilin Shen: formal analysis, writing – review & editing. Hui Yuan: formal analysis, writing – review & editing.

Conflicts of interest

The authors declare they have no financial or commercial conflicts.

Acknowledgements

The authors gratefully acknowledge the financial support of the Natural Science Foundation of Xinjiang (grant no. 2021D01A126) and the Science Fund for Excellent Young Scholars of Xinjiang Autonomous Region (grant no. 2017Q063).

References

1 X.-Z. Li, C.-B. Tia and Q.-F. Sun, *Chem. Rev.*, 2022, **122**, 6374–6458, DOI: 10.1021/acs.chemrev.1c00602.

2 R. Zhang, J. Shang, J. Xin, B. Xie, Y. Li and H. Möhwald, *Adv. Colloid Interfac.*, 2014, **207**, 361–375, DOI: 10.1016/j.cis.2013.12.012.
3 S.-Y. Wu, X.-Q. Guo, L.-P. Zhou and Q.-F. Sun, *Inorg. Chem.*, 2019, **58**, 7091–7098, DOI: 10.1021/acs.inorgchem.9b00756.
4 A. F. Y. Matsushita, A. A. C. C. Pais and A. J. M. Valente, *Colloid. Surface. A*, 2019, **569**, 93–101, DOI: 10.1016/j.colsurfa.2019.02.049.
5 H. E. Emam, H. N. Abdelhamid and R. M. Abdelhameed, *Dyes Pigm.*, 2018, **159**, 491–498, DOI: 10.1016/j.dyepig.2018.07.026.
6 G. W. Xu, Y. P. Wu, W. W. Dong, J. Zhao, X. Q. Wu, D. S. Li and Q. Zhang, *Small*, 2017, **13**, 1–8, DOI: 10.1002/smll.201602996.
7 X. Wang, T. Qin, S.-S. Bao, Y.-C. Zhang, X. Shen, L.-M. Zheng and D. Zhu, *J. Mater. Chem. A*, 2016, **4**, 16484–16489, DOI: 10.1039/C6TA06792A.
8 Q. Y. Yang, K. Wu, J. J. Jiang, C. W. Hsu, M. Pan, J. M. Lehn and C. Y. Su, *Chem. Commun.*, 2014, **50**, 7702–7704, DOI: 10.1039/C4CC01763C.
9 M. Chen, W.-M. Xu, J.-Y. Tian, H. Cui, J.-X. Zhang, C.-S. Liu and M. Du, *J. Mater. Chem. C*, 2017, **5**, 2015–2021, DOI: 10.1039/C6TC05615F.
10 B. Yan, *Inorg. Chem. Front.*, 2021, **8**, 201–233, DOI: 10.1039/D0QI01153C.
11 K. Ren, S.-H. Wu, X.-F. Guo and H. Wang, *Inorg. Chem.*, 2019, **58**(7), 4223–4229, DOI: 10.1021/acs.inorgchem.8b03284.
12 W. Liu, X. Huang, C. Chen, C. Xu, J. Ma, L. Yang, W. Wang, W. Dou and W. Liu, *Chem. – Eur. J.*, 2019, **25**(4), 1090–1097, DOI: 10.1002/chem.201805080.
13 Y. Li, M. Sun, Y. Yang, H. Meng, Q. Wang, C. Li and G. Li, *J. Mater. Chem. C*, 2021, **9**, 8683–8693, DOI: 10.1039/D1TC02042K.
14 K. Yi and L. Zhang, *Food Chem.*, 2021, **354**, 129584, DOI: 10.1016/j.foodchem.2021.129584.
15 G. Cheng, X. Li, X. Li, J. Chen, Y. Liu, G. Zhao and G. Zhu, *J. Hazard. Mater.*, 2022, **423**, 127087, DOI: 10.1016/j.jhazmat.2021.127087.
16 M. Werner, M. S. Glück, B. Bräuer, A. Bismarck and P. A. Lieberzeit, *Soft Matter*, 2022, **18**, 2245–2251, DOI: 10.1039/D2SM00137C.
17 H. Karimi-Maleh, M. L. Yola, N. Atar, Y. Orooji, F. Karimi, P. S. Kumar, J. Rouhi and M. Baghayeri, *J. Colloid Interface Sci.*, 2021, **592**, 174–185, DOI: 10.1016/j.jcis.2021.02.066.
18 Ö. S. Bölükbaşı, B. B. Yola, H. Boyacıoğlu and M. L. Yola, *Food Chem. Toxicol.*, 2022, **163**, 112994, DOI: 10.1016/j.fct.2022.112994.
19 M. L. Yola, *Chemosphere*, 2022, **301**, 134766, DOI: 10.1016/j.chemosphere.2022.134766.
20 O. Akyıldırım, F. Kardaş, M. Beytur, H. Yüksek, N. Atar and M. L. Yola, *J. Mol. Liq.*, 2017, **243**, 677–681, DOI: 10.1016/j.molliq.2017.08.085.
21 C. Karaman, O. Karaman, N. Atar and M. L. Yola, *Microchim. Acta*, 2022, **189**, 24, DOI: 10.1007/s00604-021-05128-x.
22 L. Luo, F. Zhang, C. Chen and C. Cai, *Microchim. Acta*, 2020, **187**(2), 40, DOI: 10.1007/s00604-020-4122-1.
23 N. Özcan, C. Karaman, N. Atar, O. Karaman and M. L. Yola, *ECS J. Solid State Sci.*, 2020, **9**, 21010, DOI: 10.1149/2162-8777/abd149.
24 L. Uzun, R. Uzek, S. Şenel, R. Say and A. Denizli, *Mater. Sci. Eng., C*, 2013, **33**(6), 3432–3439, DOI: 10.1016/j.msec.2013.04.032.
25 Z. Long, S. Shen, Y. Lu, W. Lan, J. Chen and H. Qiu, *Anal. Bioanal. Chem.*, 2019, **411**(18), 4221–4229, DOI: 10.1007/s00216-019-01902-2.
26 B. V. Crist, *Handbook of monochromatic XPS spectra: the elements of native oxides, XPS international*, England, John Wiley & Sons, 2000.
27 M. Muniz-Miranda, *J. Phys. Chem. A*, 2000, **104**, 7803–7810, DOI: 10.1021/jp001578y.
28 X. Ren, Q. Liu, H. Feng and X. Yin, *Appl. Mech. Mater.*, 2014, **665**, 367–370, DOI: 10.4028/www.scientific.net/AMM.665.367.
29 O. A. C. Monteiro Jr and C. Airoldi, *Int. J. Biol. Macromol.*, 1999, **26**(2–3), 119–128, DOI: 10.1016/S0141-8130(99)00068-9.
30 L. A. Diaz-Torres, E. De la Rosa, P. Salas, V. H. Romero and C. Angeles-chávez, *J. Solid State Chem.*, 2008, **181**(1), 75–80, DOI: 10.1016/j.jssc.2007.09.033.
31 S. Feng, F. Pei, Y. Wu, J. Lv, Q. Hao, T. Yang, Z. Tong and W. Lei, *Spectrochim. Acta, Part A*, 2021, **246**, 119004, DOI: 10.1016/j.saa.2020.119004.
32 J. Zhang, S. Xu, Z. Wang, P. Xue, W. Wang, L. Zhang, Y. Shi, W. Huang and R. Chen, *Angew. Chem., Int. Ed.*, 2021, **133**(31), 17231–17238, DOI: 10.1002/anie.202104361.

